ISSN: 2688-8645

Research on 3D Geometric Modeling Theory of Multi-constraint Environment for UAV Rescue after Earthquake

Xinyu Zhu, Jianyu Chu

North China University of Science and Technology, Tangshan Hebei, 063210, China

Abstract

The effectiveness of emergency response to earthquake disasters is crucial for the safety of lives and property. Unmanned Aerial Vehicles (UAVs), with their unique mobility, have emerged as a key force in reopening lifelines after earthquakes. However, the post-earthquake environment is fraught with multiple constraints, including building collapses, secondary disasters, restricted airspace, and urgent material demands, posing significant challenges to UAV path planning. To address these challenges, this research focuses on the core issue of "UAV path planning in multi-constraint environments after earthquakes." It systematically constructs a multi-level assessment index system encompassing disaster severity, demand urgency, environmental feasibility, and rescue support level, and establishes a high-fidelity 3D geographic environment model. Furthermore, an Improved Ant Colony Optimization (IACO) algorithm is proposed. By integrating a composite heuristic function that considers task priority and environmental risks, along with a dynamic pheromone update strategy, the algorithm effectively balances path economy, safety, and mission timeliness. This study aims to form a complete technical closed-loop from "environmental perception" to "intelligent decision-making," providing a solid theoretical and technical foundation for precise UAV rescue operations in complex disaster scenarios.

Keywords

Path Planning of UAV; Post-earthquake Rescue; Multi-constraint Environment; Improved Ant Colony Optimization Algorithm; 3D Geographical Modeling.

1. 3D Geometric Modeling of Post-earthquake Rescue Environment

To accurately simulate the complex post-earthquake environment and validate the UAV path planning algorithms, this study constructs a multi-constraint 3D geographic environment model integrating building clusters and mountainous flight zones[1]. The model comprehensively considers the typical characteristics of the post-earthquake environment and the practical constraints of UAV flight, providing a high-fidelity, multi-constraint simulation foundation for path planning algorithms[2].

1.1. Indicators System for Assessing Disaster Areasafter Earthquakes

The efficient delivery of drone-assisted relief supplies post-earthquake is pivotal for minimizing disaster impacts and saving lives, with its effectiveness heavily dependent on accurate and rapid assessment of disaster zones[3]. Traditional methods relying on manual surveys and macroscopic intensity evaluations fall short in meeting the demands of drone rescue command decisions regarding timeliness and precision. Therefore, establishing a scientific, systematic, and quantifiable disaster assessment index system holds critical theoretical and practical significance for achieving intelligent and precise allocation of relief resources[4]. This study draws on the framework of resilience system theory, closely aligning with the technical characteristics and operational constraints of urban low-altitude drone

ISSN: 2688-8645

logistics, to develop an assessment index system for determining disaster zones for post-earthquake drone relief supply delivery[5].

This system aims to "achieve precise and efficient delivery of rescue supplies via drones," with its core mission being to optimize resource allocation during the critical post-earthquake emergency period, ensuring essential supplies reach the most affected areas with minimal risk. To achieve this ultimate goal, the guideline framework establishes four evaluation criteria: First, "disaster severity" objectively quantifies the physical damage caused by earthquakes to vulnerable populations, which serves as the root cause of supply demand. Second, "urgency of need" identifies and measures the criticality of rescue requirements across different regions, establishing transportation priority levels[6]. Third, "environmental accessibility" specifically evaluates external constraints and risks for drone operations in target areas, forming the basis for route planning feasibility[7]. Fourth, "rescue support capacity" assesses the foundational capabilities of disaster zones in supporting drone operations—including landing, cargo handling, and communication support—which directly impacts the efficiency of rescue efforts. As shown in the table below:

Table 1. Assessment Index System for Post-Earthquake Disaster Severity

name of index	computational formula	Formula Explanation	index attribute
Building collapse density	$s_1 = \frac{N}{A} \times 100\%$	NAThe number of collapsed buildings identified by the drone, used to assess the total area of the region.	forward direction
life interruption index	$S_2 = \alpha_1 \cdot R + \alpha_2 \cdot C + \alpha_3 \cdot P$	$RCP\alpha\alpha_1 + \alpha_2 + \alpha_3 = 1$*The road network outage rate, the communication outage rate, and the water supply network outage rate; the weight coefficient*	forward direction
Secondary disaster risk level	$s_3 = p_1$	Based on factors such as seismic intensity, slope, lithology, and rainfall, the probability of occurrence is calculated using logistic regression or random forest models, and the results are classified into 1-5 levels.	forward direction

Table 2. Index System for Emergency Material Demand Urgency

name of index	computational formula	Formula Explanation	Indicator Properties
Forecasting the scale of the affected population	$D_1 = f$	The prediction values are calculated $S_1S_2S_3$by ACO-SVM prediction model based on seismic intensity, building collapse density, life interruption index and secondary disaster risk level.	forward direction
Vulnerability Index of Population	$D_2 = \beta_1 \cdot m_1 + \beta_2 \cdot m_2 + \beta_3 \cdot m_3$	$m_1, m_2, m_3\beta_1, \beta_2, \beta_3$The proportions of the elderly, children, and people with disabilities; these are the weight coefficients.	forward direction
Signs for special locations	1.0 $or D_3 = D_3 = 1.5$	The value is 1.5 if the evaluated area is a school, hospital, or emergency shelter; otherwise, it is 1.0.	forward direction
Duration of the material shortage	$D_4 = T_C - T_e$	T_CT_eCurrent time or earthquake disaster time	forward direction

Table 3. Index System for Environmental Feasibility

name of index	computational formula	Formula Explanation		Indicator Properties	
meteorologic condition	$E_1 = 0(v_s < v_{\max})$ $E_1 = 1(v_s > v_{\max})$	v_sv_{max}Wind speed for the scenario, and the drone's maximum wind resistance		negative direction	
terrain complexity	$E_2 = \frac{\sigma}{\Delta H}$	$\sigma\Delta H$is the standard deviation of elevation in the grid, and is the relative height difference. The larger the value, the higher the difficulty of passage.		negative direction	
Airspace congestion	$E_3 = \frac{N_u}{A}$	N_uATo estimate the number of drones in the airspace, for the airspace area		negative direction	
availability of take-off and landing points	$E_4 = \frac{N_L}{A_L}$	N_LA_LCalculate the average area of available takeoff and landing points.		forward direction	

ISSN: 2688-8645

The internal logical relationship between the two forms the decision-making basis of UAV rescue scheduling: an area with extremely serious disaster and high urgency demand must be the absolute priority of rescue operation.

Table 4. Index System for Rescue Support Leve

name of index	computational formula	Formula Explanation		Indicator Properties	
strength of communication signal	$R_1 = 3,2,1,0$	Classify signal strength into four levels (3: strong, 2: medium, 1: weak, 0: none) based on field tests or carrier data		forward direction	
local reception capability	$perhaps R_2 = 1 R_2 = 0$	Rescue response with and without support, binary indicator		forward direction	
electricity availability	$R_3 = 1,0.5,0$	Classified into three levels based on actual conditions: 1 (stable power), 0.5 (unstable power), and 0 (no power)		forward direction	

The comprehensive score for final requirement urgency is used to generate a demand heatmap and serves as the direct basis for prioritizing material distribution[8]. A weighted sum model of multi-dimensional indicators can be applied, as shown below:

$$D_t = [(\omega_1 \cdot D_1) + (\omega_2 \cdot D_2)] \cdot D_3 \cdot \log(\mathrm{D}_4 + 1)$$

$\omega_1, \omega_2 D_1, D_2 D_3 \log(\mathrm{D}_4 + 1)$ Normalization weights to balance scale and vulnerability[9]. As a multiplier, it directly amplifies demand in specific regions. It simulates the nonlinear growth relationship where "the longer the time, the more urgent the demand".

The comprehensive environmental passability score is used as the cost function for path planning, where higher values indicate greater flight risks and difficulties. The specific model is as follows:

$$E_t = \gamma_1 \cdot E_1 + \gamma_2 \cdot E_2 + \gamma_3 \cdot E_3 - \gamma_4 \cdot E_4$$

$\gamma_1, \gamma_{2,} \gamma_{3,} \gamma_4 E_1 E_1 = 1$ The weight coefficients for each indicator reflect the impact of different factors on passability. The variable is binary (0 or 1); if the weather is bad, it can be directly determined as impassable[10].

In summary, the multi-level evaluation index system developed in this study integrates disaster severity, urgency of needs, environmental accessibility, and rescue support capabilities. By introducing quantitative calculation formulas and dynamic weighting mechanisms, it achieves a transformation from macro qualitative assessment to micro quantitative analysis of post-earthquake disaster conditions[11]. The system deeply integrates remote sensing interpretation, predictive model outputs, and real-time monitoring data, enabling precise quantification and spatial representation of key indicators such as "building collapse density," predicted affected population scale," and "meteorological conditions." Through algorithms like "special location identification weighting" and "material shortage duration functions," it ensures scientific integration of humanitarian considerations and rescue priorities[12]. Ultimately, the structured parameter set generated by this system provides direct and reliable decision-making inputs for upper-level UAV path planning algorithms, driving the creation of flight plans that balance safety and timeliness[13]. This forms a closed-loop feedback system progressing from "multi-source perception" to "intelligent decision-making" and then to "precision execution," laying a solid theoretical and technical foundation for enhancing the accuracy, intelligence, and efficiency of post-earthquake UAV rescue operations[14].

1.2. Hierarchical Modeling Theory Model

This study employs parametric modeling methodology to construct a 1800m × 1800m × 250m (X×Y×Z) three-dimensional urban environment on the MATLAB platform, with the modeling process following a systematic logical framework:

ISSN: 2688-8645

1) Based on the principle of hierarchical modeling of environmental elements, the complex space is divided into three relatively independent layers: terrain layer, building layer, and no-fly zone layer, which are used to simulate natural terrain features, artificial building distribution, and hazardous area ranges respectively[15].
2) Through spatial discretization, continuous geographic space is transformed into a uniformly distributed grid point matrix to construct the node network topology required for path search[16].
3) The multi-constraint integration strategy is adopted to integrate the physical constraints such as building obstacles, no-fly zone boundary and terrain elevation change into the path feasibility judgment mechanism, thus forming a comprehensive environment model with both geometric authenticity and computational feasibility[17].
The terrain layer modeling is based on the theory of digital elevation model, and adopts the method of superposition of multi-peak Gaussian function to construct the three-dimensional terrain surface conforming to the real terrain characteristics. The terrain elevation function is expressed as:

$$z(x,y)=\sum_{i=1}^{N_p} A_i \cdot \left[-\frac{(x-x_i)^2+(y-y_i)^2}{2\sigma_i^2} \right] + \varepsilon(x,y)$$

The parameters N_p N_p include A_i A_i the number (x_i, y_i) of main (x_i, y_i) σ peaks, peak height σ, the coordinates $\varepsilon(x,y)$ of the mountain $\varepsilon(x,y)$ peak center, and the Gaussian standard deviation to control the slope of the peaks[18]. The random noise makes the generated terrain more natural and better tests the performance of the path planning algorithm[19].
The 3D modeling of the stratum layer is shown below:

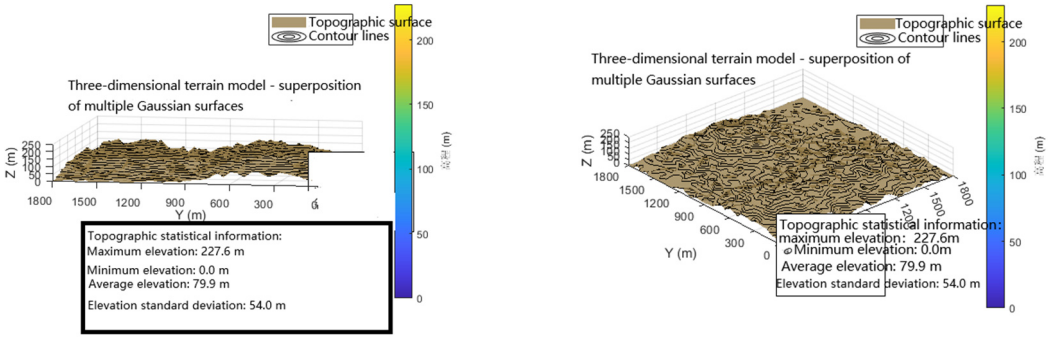

Fig 1. Terrain Layer Based on Elevation Model

The terrain grid is generated by the grid generation function with a grid point spacing of 50 meters, forming a regular grid of 37×37 points in the 1800m×1800m area, with a total of 1369 terrain sampling points[20].
The architectural modeling employs a parametric generation method based on rule-based grids to construct a dense urban area containing 300-350 buildings. The modeling process begins with grid division to establish the building layout framework, setting uniform 15m×15m square building foundations and 8m spacing between structures to ensure rational spatial distribution[21]. Building heights are randomly generated within a range of 10-120m, simulating the diversity of building heights in real-world urban environments. As shown in the figure below:

ISSN: 2688-8645

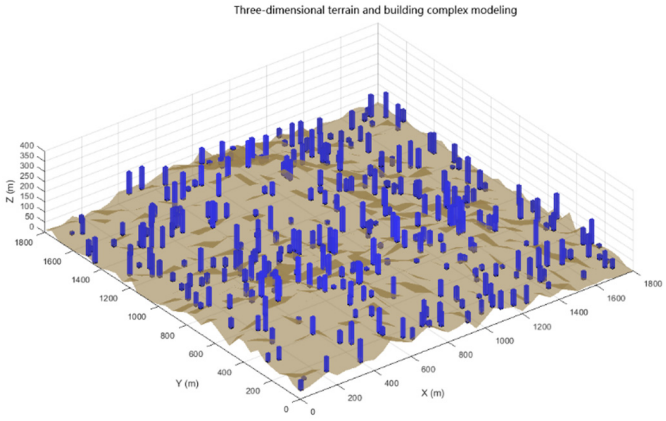

Fig 2. 3D Terrain and Building Complexes

Flight prohibition layer modeling is a critical component in post-earthquake UAV path planning, grounded in airspace management theory and risk assessment methodologies[22]. These zones designate high-risk or strictly restricted areas post-disaster, including but not limited to: fire zones, chemical spill sites, severely collapsed structures, emergency rescue core zones, and any areas potentially compromising drone flight safety[23].

The no-fly zone (NFAZ) modeling employs a parametric stochastic generation method to create 6-10 cubic NFAZs within a 1800m×1800m area, with dimensions ranging from 100-300m (length and width) and 50-120m (height), simulating hazardous zones such as post-earthquake fires and collapses. A spatial constraint algorithm ensures safe distances between NFAZs and the starting/ending points[24]. The geometric model uses red translucent cubes for visualization, integrated with an AABB bounding box collision detection mechanism[25].

The modeling method provides reliable safety constraints for path planning algorithm by strict parameter control and geometry optimization, which reflects the systematic modeling idea from disaster scene analysis to mathematical representation[26].

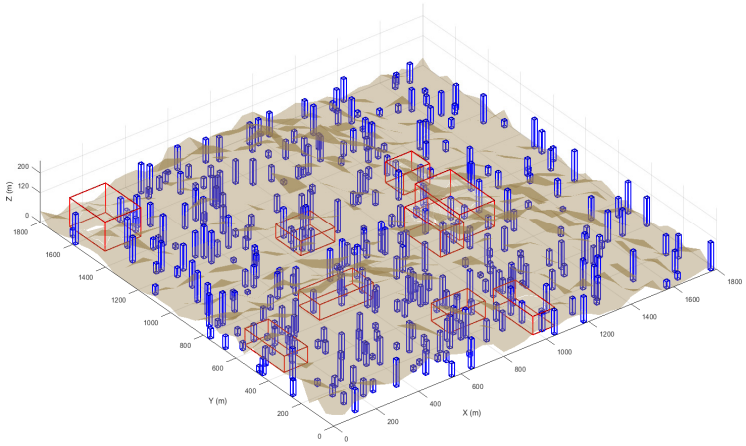

Fig 3. 3D Modeling of the No-Fly Layer

2. Theoretical Model Establishment

This study establishes a multi-level evaluation index system that integrates disaster severity, urgency of needs, environmental accessibility, and rescue support capabilities, providing a quantitative basis for drone rescue route planning. Building on this foundation, this section further develops a theoretical model for route planning, aiming to translate the aforementioned

ISSN: 2688-8645

predictions and assessments into actionable drone flight plans, thereby forming an integrated "prediction-assessment-planning" research framework[27].

2.1. Problem Description and Basic Assumptions

China is a country with frequent seismic activity. Despite occupying only 7% of the global land area, it has experienced 33% of the world's earthquakes, which further highlights the severity of earthquake disasters. According to statistics from the China Earthquake Information Network, in the 20th century, China experienced 380 earthquakes of magnitudes 6.0 to 6.9, 65 earthquakes of magnitudes 7.0 to 7.9, and 7 earthquakes of magnitudes 8.0 or higher, including 2 earthquakes of magnitude 8.5. Earthquakes have caused enormous losses to the lives and property of the Chinese people[28].

The post-earthquake emergency rescue environment is highly complex, primarily manifested in three aspects: First, infrastructure is severely damaged, road networks are disrupted, and traditional transportation methods struggle to effectively carry out rescue operations. Second, disaster areas contain numerous secondary hazard zones, such as fire zones and collapsed areas, which pose threats to drone flight safety. Third, the demand for rescue supplies exhibits significant spatiotemporal heterogeneity, with varying urgency levels across different affected areas[29]. These characteristics make drone path planning a classic multi-objective, multi-constraint optimization problem.

To address this complex decision-making environment, the study establishes the following fundamental assumptions: First, the disaster zone's geographical layout can be discretized into a two-dimensional grid map, with each grid cell representing a decision node. Second, the rescue system comprises a logistics hub (starting point) and multiple affected locations (endpoints), where the urgency of material demands at each endpoint is predetermined[30]. Third, the environment contains designated high-risk zones that drones must strictly avoid. Fourth, drones operate at constant speeds while adhering to predefined altitude and speed constraints. Fifth, drones can independently plan their routes without any coordination conflicts.

2.2. Construction of Multi-objective Optimization Function

Based on the problem description and basic assumptions, this study constructs a multi-objective optimization model with three core objectives: minimizing flight distance, threat cost, and altitude cost. Considering that multi-objective optimization problems typically lack a single optimal solution but rather a Pareto optimal solution set, the study employs the weighted sum method to transform the multi-objective problem into a single-objective problem for resolution[31].

The core objective function of the model is defined as follows:

$$\min F = \sum_{a=1}^{N} \sum_{(i,j)\in\varepsilon} (w_1 L_{ij} + w_2 T_{ij} + w_3 H_{ij}) x_{ij}^{a}$$

The total L flight distance is the cost of the path economy T , the threat cost is the cost of the H path safety H , and the altitude cost is the cost of the flight w_1、w_2、w_3 altitude w_1、w_2、w_3 on the $w_1+w_2+w_3=1$ energy consumption and stability $w_1+w_2+w_3=1$.

The weight coefficients are determined by fully incorporating the material demand urgency information predicted in Section For regions with higher demand urgency, the time weight is appropriately increasedto ensure rapid delivery of relief supplies. For areas with complex terrain and higher risks, the safety weight is correspondingly enhanced to guarantee flight safety. This dynamic weight adjustment mechanism reflects a paradigm shift from "geometric path optimization" to "rescue mission optimization".

ISSN: 2688-8645

The decision x_{ij}^{a} variable is a binary variable a, indicating i whether j the $x_{ij}^{a}=1$ drone chooses $x_{ij}^{a}=1$ $x_{ij}^{a}=0$ path from node to $x_{ij}^{a}=0$ node. When, it means the path is selected; when, it means the path is not selected. Through this definition of the variable, the continuous path planning problem is transformed into a discrete network optimization problem[32].

2.3. Design of the Constraint System

In post-earthquake UAV rescue path planning, the design of constraint conditions directly impacts the feasibility, safety, and practicality of the routes. This study establishes a comprehensive constraint system based on the unique post-earthquake environment and technical requirements for UAV flight[33]. The system encompasses four dimensions: path structure constraints, physical performance constraints, regional safety constraints, and timeliness constraints. This ensures the planning solution not only meets mathematical optimization requirements but also fulfills practical rescue needs.

1. Path structure constraints

Path structure constraints ensure the integrity of rescue missions and the continuity of routes, serving as fundamental constraints in path planning. The starting point departure constraint guarantees that every drone departs from a designated logistics hub, mathematically expressed as:

$$\sum_{j} x_{sj}^{a}=1 \quad \forall a\in\{1,2,...,N\}, s\in S$$

The constraint S on the starting point set ensures all drones can take off for rescue missions. The arrival constraint guarantees each drone ultimately reaches the designated disaster site[34].

$$\sum_{i} x_{ie_a}^{a}=1 \quad \forall a$$

This indicates the drone's target destination, ensuring rescue supplies are delivered precisely to the intended area. The intermediate node flow balance constraint guarantees path continuity and loop-free operation, preventing any stops or loops at intermediate nodes.

$$\sum_{i} x_{ik}^{a}=\sum_{j} x_{ik}^{a} \quad \forall k\notin S\cup E, \forall a$$

This constraint ensures that the UAV immediately moves to the next node after completing the current node task, thus improving rescue efficiency[35].

2. Physical performance constraints

Physical performance constraints account for the actual flight capabilities and hardware limitations of the UAV. The flight speed constraint defines the maximum allowable flight speed of the UAV:

$$v_{ij}^{a}\le v_{\max} \quad \forall(i,j), \forall a$$

The flight $v_{\max}$ time constraint is determined based on the selected drone model (e.g., the DJI Matrice350 RTK has a maximum speed of 23 m/s). This constraint takes into account the battery's endurance[36].

$$\sum_{(i,j)} t_{ij}^{a}\le T_{\max} \quad \forall a$$

The maximum $T_{\max}$ $T_{\max}$ endurance of the drone is approximately 55 minutes for the Matrice350 RTK under full load conditions. Flight altitude constraints ensure flight safety:

$$h_{\min}\le h_{ij}^{a}\le h_{\max} \quad \forall(i,j), \forall a$$

ISSN: 2688-8645

This constraint prevents the drone from flying too low (collision risk) or too high (signal loss risk), typically setting a minimum safe altitude of 30 meters above the ground and a maximum flight altitude of 500 meters.

3. Regional security constraints

Regional safety constraints are critical requirements in post-earthquake environments, directly impacting drone flight safety. The no-fly zone regulations in high-risk areas prohibit all flight paths from crossing hazardous zones.

$$x_{ij}^{a} = 0 \quad \text{if} (i,j) \cap M \neq 0$$

This represents M $M$the set of all high-risk areas (e.g., fire, collapse, chemical spill zones). The dynamic risk zone constraint accounts for the impact of aftershocks and secondary disasters.

$$x_{ij}^{a}(t) = 0 \quad \text{if} \quad \mathrm{R}_{ij}(t) > R_t$$

The risk $\mathrm{R}_{ij}(t)$ $\mathrm{R}_{ij}(t)$ t value (i,j) t at (i,j) the moment path is indicated, which can be dynamically updated based on the aftershock prediction model and real-time monitoring data. The communication support constraint ensures the drone remains within a controllable range at all times.

$$d_{ij}^{a} \leq d_c \quad \forall (i,j), \forall a$$

The maximum d_c d_c communication range is approximately 7-10 kilometers for conventional drones.

4. Time-bound constraints

The timeliness constraint reflects the urgency of post-earthquake rescue. The golden rescue time constraint requires that supplies be delivered within 72 hours.

$$\sum_{(i,j)} t_{ij}^{a} \leq 72h \quad \forall a$$

The urgency priority constraint ensures that high urgency areas are prioritized for rescue:

$$\sum_{a} \sum_{(i,j)} x_{ij}^{a} \cdot U_e \geq U_{\min} \quad \forall \mathrm{e} \in E_h$$

This represents U_e U_e ethe eurgency E_h level E_h of affected points, forming a set of high-priority disaster sites. The time window constraint considers the optimal rescue timing for different affected points.

$$t_e \in \left[T_e^{\min}, T_e^{\max} \right] \quad \forall \mathrm{e} \in E$$

The earliest $T_e^{\min}$ $T_e^{\max}$ $T_e^{\min}$ $T_e^{\max}$ and ethe latest erescue time of the disaster site are indicated by and.

5. Load capacity constraints

The payload capacity constraint considers the material transportation capability of the UAV. The weight constraint limits the weight of materials transported in a single mission.

$$\sum_{e} w_e \cdot y_e^{a} \leq W_{\max} \quad \forall a$$

This w_e indicates w_e the e maximum $W_{\max}$ e payload $W_{\max}$ capacity of the drone for delivering supplies to disaster areas. The volume constraint limits the total volume of transported materials.

$$\sum_{e} v_e \cdot y_e^{a} \leq V_{\max} \quad \forall a$$

ISSN: 2688-8645

This indicates v_e v_e the volume $ee$of supplies $V_{\max}$ $V_{\max}$ delivered to disaster areas, which is the maximum capacity of the drone.

This constraint system ensures both feasibility and safety of path planning across multiple dimensions, providing clear boundary conditions for subsequent algorithm implementation. The comprehensive design of this constraint framework not only maintains the rigor of the mathematical model but also guarantees the applicability and reliability of the planning solution in real-world rescue scenarios. This establishes a solid foundation for the algorithm design and simulation validation detailed in next Section [37].

3. UAV Path Planning Based on Improved Ant Colony Optimization (IACO) Algorithm

Building upon the multi-objective optimization model and constraint framework developed in Section 3.2, and considering the critical characteristics of post-earthquake rescue scenarios—prioritizing urgency and dynamic constraint adaptation—we propose targeted enhancements to the traditional Ant Colony Optimization (ACO) algorithm. This results in the Improved Ant Colony Optimization (IACO) algorithm, which integrates disaster prediction, environmental constraints, and task adaptation. Simulation experiments validate IACO's effectiveness in post-earthquake UAV path planning. The specific implementation details are as follows:

3.1. Improving the Core Mechanism Design of Ant Colony Optimization (IACO) Algorithm

The traditional ACO algorithm has some defects in post-earthquake scene, such as single heuristic information, easy saturation of pheromone, and poor adaptability of multi-constraint. This paper improves the algorithm from three aspects, such as constructing composite heuristic function, updating strategy of dynamic pheromone, and mediation mechanism of multi-constraint conflict, and forms the core logic of the algorithm suitable for post-earthquake rescue[38].

Breaking away from the conventional ACO's reliance on the singular guidance of "inverse (D_t) distance (E_t)," this (E_t) approach (H_{ij}) incorporates (H_{ij}) the urgency of quantized requirements, environmental passability, and terrain elevation costs from Section 3.1.3 into the heuristic function. This creates a multi-factor collaborative guidance mechanism that ensures path planning simultaneously meets the requirements of "timeliness, safety, and task priority." The specific formula is as follows:

$$\eta_{ij} = w_1 \cdot \frac{1}{L_{ij} + \varepsilon} + w_2 \cdot D_j + w_3 \cdot (1 - E_{ij}) + w_4 \cdot \frac{1}{H_{ij} + \varepsilon}$$

In addition, the weight distribution $(w_1 - w_4)$ $(w_1 - w_4)$ was determined by the analytic hierarchy process (AHP) combined $w_1 = 0.3$ with the $w_1 = 0.3$ $w_2 = 0.4$ priority of $w_2 = 0.4$ $w_3 = 0.2$ post $w_4 = 0.1$-earthquake relief $w_3 = 0.2$, in $w_4 = 0.1$ which the "golden 72 hours" took (distance cost), (demand urgency), (environmental safety), (altitude cost), and the priority was to ensure the delivery of materials to high-demand areas.

The hybrid heuristic function is integrated into the ant's state transition decision, expressed as:

$$p_{ij}^k(t) = \frac{\left[\tau_{ij}(t)\right]^{\alpha} \cdot \left[\eta_{ij}\right]^{\beta}}{\sum_{s \in allowed_k} \left[\tau_{ij}(t)\right]^{\alpha} \cdot \left[\eta_{is}\right]^{\beta}}$$

ISSN: 2688-8645

The pheromone $t\ \tau_{ij}(t)\ i$ concentration $j\ j\ i$ from $\alpha=1.2$ the time $\alpha=1.2$ node to the node is (pheromone $\beta=3.5$ importance coefficient $\beta=3.5$, controlling the balance between $allowed_k$ exploration k and utilization $allowed_k$ of k the algorithm), (heuristic information importance coefficient, strengthening the guiding role of the demand and environment); the feasible neighbor node set of the ant is (excluding the visited node and high-risk no-fly zone).

To solve the problems of easy saturation and slow convergence of traditional ACO, a three-layer pheromone update mechanism of "global volatilization + elite feedback + demand weighting" is designed, which avoids the algorithm falling into local optimum and strengthens the guidance of high-demand path.

After each iteration, all pheromone on the path is fixed proportion volatilization, the formula is:

$$\tau_{ij}(t+1)=(1-\rho)\cdot\tau_{ij}(t)$$

The volatility $\rho=0.12$ coefficient surpasses that 0.1 of traditional 0.1 ACO, which enhances the algorithm's dynamic exploration capability and adapts to emergencies like post-earthquake aftershocks and secondary disasters.

In each iteration, elite ants that satisfy the criteria of "path length ≤ 80% of average length, no collision risk, and coverage of high-demand nodes ≥ 3" are selected, with additional pheromon e added to their paths. The formula is:

$$\tau_{ij}(t+1)=\tau_{ij}(t+1)+\frac{Q_e}{L_e}$$

The elite $Q_e=150$pheromone intensity is L_e higher than L_e that of ordinary ants. The path length of elite ants (unit: m) is used to accelerate the convergence ofhigh-quality paths.

For paths passing through $(D_j\geq 4)$ "high-demand nodes", The formula is:

$$\tau_{ij}(t+1)=\tau_{ij}(t+1)\cdot(1+0.2\cdot D_j)$$

The mechanism guides the ants to choose the path of high demand area first, and realizes the dynamic binding of "demand priority-path planning."

To ensure the planned path meets both feasibility and safety requirements, this study implements a three-tiered multi-constraint conflict resolution mechanism integrating Section 3.2.3's physical performance constraints (speed, endurance, altitude) with regional safety constraints (no-fly zones, risk zones). During the pre-detection phase, the system employs an AABB bounding box collision detection method (compatible with irregular obstacles like 3D structures and mountains) to conduct multi-dimensional feasibility verification of candidate paths. The verification includes: 1) Spatial safety validation: Ensuring the minimum distance between the path and obstacles (e.g., buildings, mountains) meets a 20m safety threshold, and avoiding high-risk no-fly zones (e.g., areas with wind speeds exceeding the drone's maximum wind resistance of 12m/s, or regions with secondary disaster risk level ≥4);

2) Physical performance validation: Assessing whether the remaining endurance time (55 minutes under full payload) and altitude changes (≤0.8m/s maximum climb rate) meet operational requirements. If any validation fails, the path is marked as "unfeasible" and excluded from the drone's viable neighbor node set.

During the dynamic avoidance phase, when the algorithm encounters local trapping scenarios (e.g., dense building clusters or multiple no-fly zones overlapping to reduce viable neighbor nodes to ≤3), the "virtual sub-target" compensation mechanism activates. Using the current node-target disaster point line as the reference axis, a virtual node is generated at 200m from the current node and 30m above terrain elevation. This virtual node is incorporated into the

ISSN: 2688-8645

viable neighbor set, enabling path breakthrough through "step-by-step guidance" to prevent algorithmic convergence failure due to local constraints[39].

During the path correction phase, the initially planned route undergoes smoothing and optimization. If the path exhibits vertical fluctuations exceeding 50 meters (which surpasses the drone's maximum climbing capability), the system applies k-order B-spline curves[40].

$$P(u) = \sum_{i=0}^{n} N_i, k(u) P_i$$

The system $N_i, k(u)$ k employs P_i k a B-spline P_i basis function to smooth path segments, ensuring elevation gradients remain ≤0.5m/m. It merges redundant nodes (adjacent nodes within 50m without constraint differences) to reduce path length without compromising safety, optimizing for endurance constraints. This three-tier mechanism—combining preventive measures, real-time mediation,and post-incident optimization—effectively resolves multi-constraint conflicts, guaranteeing safe and efficient drone operations in post-earthquake complex environments[41].

3.2. Algorithm Simulation Experiment Design

To validate the effectiveness of the Improved Ant Colony Optimization (IACO) algorithm in post-earthquake UAV rescue logistics path planning, this study developed a simulation environment on MATLAB R2023a platform. Using Section 3.1 disaster assessment data and Section 3.2 constraint system as inputs, we designed a three-tier experimental framework comprising "basic performance verification, multi-scenario comparison, and constraint sensitivity analysis" to comprehensively evaluate the algorithm's efficiency, safety, and task adaptability.

The experimental geographical environment is based on the typical geomorphological features of the high-frequency earthquake zones in western China, such as the Longmenshan fault zone in Sichuan and the eastern section of the Nantian Mountains in Xinjiang. A 1800m×1800m×200m (X×Y×Z) three-dimensional post-earthquake scene model is constructed.

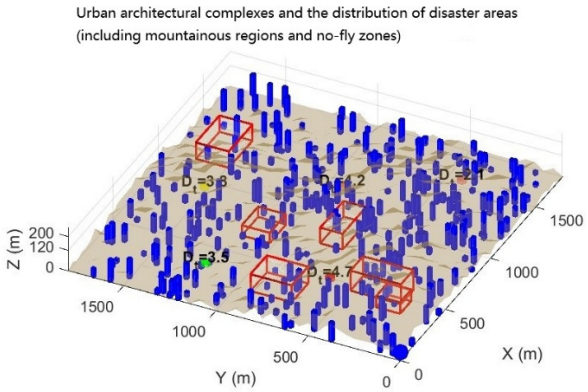

Fig 4. Post-Earthquake Environmental Simulation Map

The simulation covers 320 buildings ranging from 10 to 130 meters in height, with partial collapse structures modeled after the earthquake. It includes three mountainous terrain areas reaching 200 meters in elevation, slopes between 15° and 30°, and eight high-risk no-fly zones measuring 100-300m×100-300m D_t ×50-120m, corresponding to secondary disaster zones such as fire areas and chemical spill zones. A material distribution center and five disaster-affected endpoints are established, with their coordinates determined by post-earthquake

ISSN: 2688-8645

population density distribution, assigned urgency levels of 2.1, 3.5, 4.2, 3.8, and 4.7 respectively. As shown in the figure 4.

Table 5. Distribution of Urgency Degree for Disaster-Affected Sites

order number	Coordinate position	urgency of D_t need	area type	Supplies
1	(450, 600)	4.7	hospital	first aid medicine, blood
2	(1200, 900)	4.2	school	Food, drinking water
3	(900, 1500)	3.8	residential quarters	Tents, warm supplies
4	(300, 1200)	3.5	community	Emergency lighting equipment
5	(1500, 400)	2.1	mildly damaged area	General supplies

The drone parameters were selected from the DJI Matrice350 RTK model, a standard choice for post-earthquake rescue operations. Its physical specifications include: maximum flight speed of 23 m/s, full-load endurance of 55 minutes, maximum wind resistance of 12 m/s, minimum flight altitude of 30m (above ground), and maximum climb rate of 0.8 m/s, ensuring the simulation closely mirrors real rescue scenarios. The DJI Matrice350 RTK drone was chosen for its post-earthquake rescue applications, with parameters referencing its official technical specifications as follows:

Table 6. Reference for DJI Matrice 350 RTK Drone Parameters

Parameter category	**Parameter name**	**short-cut process**
physical property	ceiling altitude	23m/s
	full load endurance	55min
	maximum load	15kg
	maximum wind resistance	12m/s
flight constraint	minimum flight altitude	30m
	maximum altitude	500m
	maximum climb ratio	0.8m/s
ability to communicate	maximum communication distance	10km

Building upon the traditional ant colony algorithm, this study introduces a multi-factor composite heuristic function that integrates material urgency, environmental passability, and terrain elevation costs to comprehensively guide the path search process. The proposed improved ant colony algorithm (IACO) incorporates a dynamic pheromone update mechanism, combining global volatilization, elite ant strategies, and demand weight feedback to effectively balance exploration and exploitation capabilities while preventing premature convergence.

In this study's MATLAB simulation system, the IACO algorithm serves as the core path planning method. By introducing a multi-factor heuristic function and a dynamic pheromone update mechanism, it significantly enhances the performance of the traditional ant colony algorithm in complex post-earthquake environments. The experimental simulation results are shown in the figure below:

Simulation results show that IACO algorithm is superior to traditional methods in path length, convergence speed and task completion rate, especially in high-demand priority areas, which provides reliable path planning support for post-earthquake UAV material delivery.

ISSN: 2688-8645

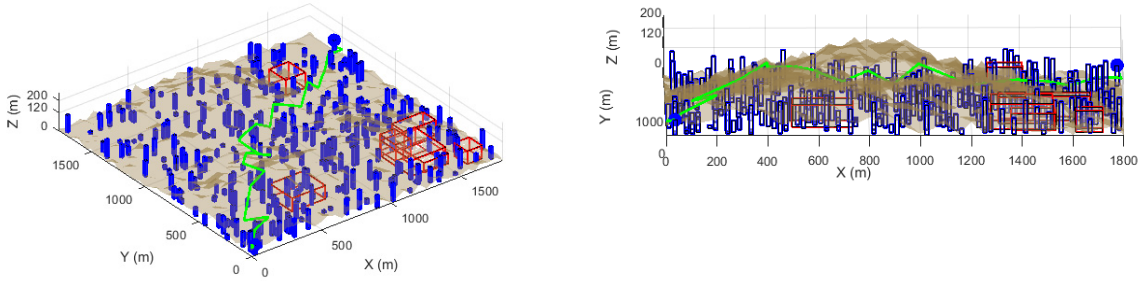

Fig 5. Path Generated by the AICO Algorithm

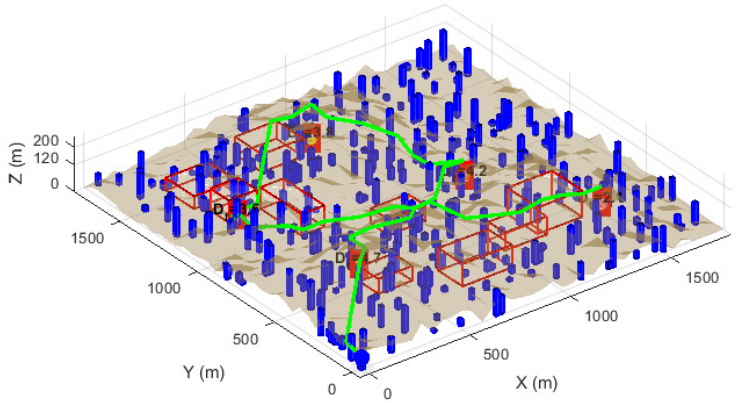

Fig 6. Path Generated by the AICO Algorithm Based on Urgency Degree

References

[1] Yang Yanming, Zhao Yun, Shao Zhufeng, et al. Research on Disruptive Technology Strategies in the Field of Mechanical and Vehicle Engineering[J].Chinese Academy of Engineering,2018,20(06):27-33.

[2] Chen Qixu, Wang Qunjing, Qian Zhe, et al. Review of technical routes and power systems of small all-electric/hybrid aircraft[J].Journal of Electrical Engineering of China,2024,44(12):4966-4986.DOI:10.13334/j.0258-8013.pcsee.222487.

[3] Xue Ling, Sun Xintong, Pan Su. Basic support, key areas and development priorities of our country's low-altitude economy[J/OL].Social Sciences Journal,1-10[2025-03-22].

[4] Gao Zhihong. Construction of Regulatory Rules for Low-altitude Flight Safety under the Concept of Equal Emphasis on Development and Safety[J/OL].2025,(03):32-46[2025-03-22].

[5] Xue Ling, Sun Xintong, Pan Su. Basic support, key areas and development priorities of our country's low-altitude economy[J/OL].Social Sciences Journal,1-10[2025-03-22].

[6] ZHANG Yanggang, LI Chengxun. Journal of the Party School of the Fujian Provincial Committee of the Communist Party of China (Fujian Institute of Administration), 2025, (01):123-129.

[7] He Chenhui. Low-altitude economy: industrial layout gradually deepening [J]. Zhongguancun, 2025, (01):28-29.

[8] Wang Gai. Research on the Opportunities, Challenges and Improvement Paths of Low-altitude Economic Development Empowering the Traditional Civil Aviation Transportation Industry[J]. China Business Review,2025,34(04):142-145.

[9] Shen Yingchun, Zhao Yuhan, Zhou Xinyi. Logical Framework and Strategic Path of Low-altitude Economic Modernization Industrial System Construction[J/OL].Jiangsu Social Sciences,1-9[2025-03-22].

[10] Ding Jie, Wang Di. Urban low-altitude UAV path planning based on reinforcement learning [J/OL]. Journal of Transportation Engineering and Information Technology,1-22[2025-03-22].

[11] Hughes L . Drone manufacturer gets FAA approval for operations over humans, moving vehicles[J]. Urgent Communications,2025.

[12] Anken T ,Coupy G ,Dubuis H P , et al. Plant protection treatments in Switzerland using unmanned aerial vehicles: regulatory framework and lessons learned. [J]. Pest management science,2025.

[13] Research on UAV track planning based on swarm intelligence algorithm[D].Hebei University of Science and Technology,2020.

[14] Research on trajectory planning of UAV and general aviation collaborative search and rescue [D]. Nanjing University of Aeronautics and Astronautics,2021.

[15] Hamid Seridi,Mohamed Amine Ferrag,Aymen Dia Eddine Berini.A new static path planning strategy for drones [J]. Internet Technology Letters,2022

[16] Deng Fei, Dou Aixia, Yuan Xiaoxiang. Application of light and small UAV in the investigation of building structure types[J].Earthquake Disaster Defense Technology,2017,12(04):786-796.

[17] Wang J ,Zhao Z ,Zheng Y . NFTSM-based Fault Tolerant Control for Quadrotor Unmanned Aerial Vehicle with Finite-Time Convergence * * This work is supported by the National Natural Science Foundation of China (No. 61573050) the open-project grant funded by the State Key Laboratory of Synthetical Automation for Process Industry at the Northeastern University (No. PAL-N201702) and CERNET Innovation Project (NGII20170803). [J]. IFAC PapersOnLine,2018,51(24):441-446. Humanitarian Shelter and Settlements Guidelines[S]. European Commission（EU）, 2017.

[18] ZHU Qing, Han Huipeng, YU Jie. Multi-objective Optimal Scheduling Method for Emergency Surveying and Mapping UAV Resources[J].Journal of Wuhan University(Information Science Edition), 2017:111-118.

[19] Zhang Zhongfeng, Gao Yunfeng, Baoyin He Xi. Hypersonic Aircraft Trajectory Planning Based on Particle Swarm Optimization[J].Journal of System Simulation,2009,21(08):2428-2431.

[20] Wei Ling, Yang Hongwei. Radio Communication Technology,2023,49(04):725-732.Sheltering Handbook [S]. American Red Cross (ARC), 2012.

[21] Li Tingzhen, Zhao Qijun, Zhang Xiayang, et al. Three-dimensional track planning of unmanned helicopter based on improved artificial potential field method[J].Flight Mechanics,2022,40(01):69-75.DOI:10.13645/j.cnki.f.d.20211210.008.

[22] Zhang Qi, Ma Jiachen, Xie Wei, et al. Journal of Northeastern University(Natural Science Edition), 2013, 34(11):1521-1524.Mega-shelter Planning Guide[S]. International Association of Venue Managers (IAVM), American Red Cross(ARC), 2010.

[23] Bagherian M, Alos A. 3D UAV trajectory planning using evolutionary algorithms: A comparison study. The Aeronautical Journal (1968). 2015; 119(1220):1271-1285.

[24] Gu Guoliang. Research on Earthquake Disaster Simulation System Based on 3D GIS Technology[D]. Beijing: Institute of Earthquake Prediction, China Earthquake Administration, 2012.

[25] Wang Sun Xiao. Research on the application of UAV in earthquake rescue and disaster relief [J]. Digital Users,2020(42):139-141

[26] Exploration on the application of UAV fleet collaborative search and rescue technology and equipment in disaster rescue[J]. China Disaster Reduction, 2023(10):42-45. DOI:10.3969/j. issn. 1002-4549.2023.10.013.

[27] Li Aijun, Li Wei. Research on the Application of UAV Technology in Environmental Monitoring[J]. Low Carbon World,2020,10(7):15,17.

[28] Exploration on the application of UAV fleet collaborative search and rescue technology and equipment in disaster rescue[J]. China Disaster Reduction, 2023(10):42-45.

[29] Otto A, Agatz N, Campbell J, Golden B, Pesch E. Optimization approaches for civil applications of unmanned aerial vehicles (UAVs) or aerial drones: A survey. Networks. 2018; 72: 411–58.

[30] Silvagni, M., Tonoli, A., Zenerino, E., & Chiaberge, M. (2016). Multipurpose UAV for search and rescue operations in mountain avalanche events. Geomatics, Natural Hazards and Risk, 8(1), 18–33.

[31] Idris F N ,Ahmad A M ,Kahlid D M , et al. UAV Thermal Imaging for Solar Panel Assessment[J]. IOP Conference Series: Earth and Environmental Science,2025.

ISSN: 2688-8645

[32] ZHAO Xuliang, HUANG Huan, CHEN Weizhi, et al. Optimal Operating Frequency Selection Method for Wireless Underground Sensor Network with Communication Constraints[J].Automation and Instrumentation,2024,(01):206-209+213.DOI:10.14016/j.cnki.1001-9227.2024.01.206.

[33] Ye Xi, Kuang Honghai. Estimation of vegetation restoration of Wangjiayan landslide after Wenchuan earthquake based on multitemporal Landsat data[J].Journal of Southwest University(Natural Science Edition),2022,44(06):150-159.DOI:10.13718/j.cnki.xdzk.2022.06.016.

[34] Li. China Equipment Engineering,2024,(22):43-45.

[35] Holzmann, P.,Wankmüller, C.,Globocnik, D.andSchwarz, E.J.(2021), "Drones to the rescue? Exploring rescue workers' behavioral intention to adopt drones in mountain rescue missions", International Journal of Physical Distribution & Logistics Management, vol. 51 no. 4, pp. 381-402.

[36] Anonymous . Military and Technical Co-operation; Russian experts to go to Italy to evaluate stability of buildings in quake zone[J]. Interfax : Russia & CIS Military Daily,2009.

[37] Elias, M., Kehl, C. and Schneider, D., 2019. Photogrammetric water level determination using smartphone technology. Photogrammetric Record, 34(166): 198–223.

[38] Jian Wang, Rui Jia, Jing Liang, Chen She, Yi-Peng Xu,Evaluation of a small drone performance using fuel cell and battery; Constraint and mission analyzes,Energy Reports,Volume 7,2021.

[39] Jack Montgomery, Gabriel Candia, Anne Lemnitzer, Alejandro Martinez,The September 19, 2017 Mw 7.1 Puebla-Mexico City earthquake: Observed rockfall and landslide activity,Soil Dynamics and Earthquake Engineering,Volume 130,2020.

[40] Emad Alfaris, R., Vafakhah, Z., & Jalayer, M. (2023). Application of Drones in Humanitarian Relief: A Review of State of Art and Recent Advances and Recommendations. Transportation Research Record, 2678(7), 689-705.

[41] Mualla Y, Najjar A, Daoud A, Galland S, Nicolle C, Shakshuki E. Agent-based simulation of unmanned aerial vehicles in civilian applications: a systematic literature review and research directions. Future Gener Comput Syst. 2019; 100: 344-364.